eng

MDPI

Article

Effect of Imposed Shear During Oval-Caliber Rolling on the Properties of Mn–Si Low-Alloy Steel

Kairosh Nogayev [1,*], Maxat Abishkenov [1], Zhassulan Ashkeyev [1], Gulzhainat Akhmetova [2], Saltanat Kydyrbayeva [1] and Ilgar Tavshanov [1]

[1] Department of Technological Machines and Transportation, Karaganda Industrial University, Temirtau 101400, Kazakhstan; m.abishkenov@tttu.edu.kz (M.A.); zh.ashkeyev@tttu.edu.kz (Z.A.); s.kydyrbayeva@tttu.edu.kz (S.K.); i.tavshanov@tttu.edu.kz (I.T.)

[2] Department of Metallurgy and Materials Science, Karaganda Industrial University, Temirtau 101400, Kazakhstan; g.akhmetova@tttu.edu.kz

* Correspondence: k.nogayev@tttu.edu.kz

Abstract

The present study examines the effect of a modified oval–round rolling scheme incorporating inclined oval calibers on the mechanical behavior and microstructural evolution of Mn–Si low-alloy steel (25G2S). Cylindrical billets were hot rolled through both classical and modified sequences under identical thermal and kinematic conditions. Tensile testing demonstrated that, relative to the unrolled condition ($\sigma_{0.2} \approx 269$ MPa; $\sigma_u \approx 494$ MPa), the classical route increased yield and ultimate strengths to ~444 MPa and ~584 MPa, respectively, whereas the modified scheme yielded comparable values (~433 MPa and ~572 MPa) while providing superior ductility ($\delta \approx 26.8\%$, $\psi \approx 68.6\%$). Vickers microhardness decreased systematically from 244 HV (unrolled) to 213 HV (classical) and 184 HV (modified), with the modified scheme exhibiting the lowest scatter ($\pm$4.8 HV), confirming enhanced structural uniformity. Scanning electron microscopy revealed ferrite–pearlite refinement under both rolling sequences, with the modified scheme producing finer equiaxed ferrite grains (~3–5 μm) and attenuated longitudinal banding. These features are indicative of shear-assisted dynamic recrystallization, activated by the inclined oval calibers. The findings highlight that the modified rolling strategy achieves a favorable strength–ductility balance and improved homogeneity, suggesting its applicability for advanced thermomechanical processing of low-alloy steels.

Keywords: Mn–Si low-alloy steel; oval–round rolling; inclined oval calibers; dynamic recrystallization (DRX); strength–ductility balance; microhardness; ferrite–pearlite morphology

check for updates

Academic Editor: Tomasz Lipiński

Received: 8 September 2025
Revised: 26 September 2025
Accepted: 29 September 2025
Published: 4 October 2025

Citation: Nogayev, K.; Abishkenov, M.; Ashkeyev, Z.; Akhmetova, G.; Kydyrbayeva, S.; Tavshanov, I. Effect of Imposed Shear During Oval-Caliber Rolling on the Properties of Mn–Si Low-Alloy Steel. *Eng* **2025**, *6*, 265. https://doi.org/10.3390/eng6100265

Copyright: © 2025 by the authors. Licensee MDPI, Basel, Switzerland. This article is an open access article distributed under the terms and conditions of the Creative Commons Attribution (CC BY) license (https://creativecommons.org/licenses/by/4.0/).

1. Introduction

The development of metallurgy and mechanical engineering is currently accompanied by increasingly stringent demands on the performance properties of both structural and functional materials. Enhancing strength, wear resistance, corrosion resistance, and component durability is impossible without deliberate control over the structural and phase state of metals and alloys. In this context, technologies based on severe plastic deformation (SPD) have received considerable attention due to their ability to achieve profound structural modification of materials.

SPD techniques encompass a suite of pressure-processing methods that yield ultrafine-grained (UFG) materials. A key attribute of these technologies is their capacity

to impose extremely high deformation levels without causing fracture of the workpiece, resulting in dramatic grain refinement and, consequently, substantial enhancement of the comprehensive mechanical properties of the material [1,2].

Numerous studies have demonstrated that the principal mechanism driving structural transformations during severe plastic deformation (SPD) involves shear deformations, particularly the simple shear mode. This deformation regime promotes intense dislocation accumulation, substructure formation, and progressive grain fragmentation, thereby creating favorable conditions for the development of stable ultrafine-grained (UFG) microstructures. As highlighted by Segal, "simple shear provides the optimal mode for structure modification and grain refinement," offering superior performance compared to pure shear in this context [3].

The recognition of simple shear's critical role in generating UFG states underscores the necessity of integrating corresponding deformation mechanisms into industrial metal forming processes. Rolling, as a fundamental plastic deformation technique, offers a particularly effective platform for this integration.

Conventional longitudinal rolling predominantly involves plane–strain compression, which limits achievable grain refinement and impedes property enhancement without risking workpiece failure. However, incorporating shear components into the rolling process has significantly expanded its potential. Advanced rolling techniques—such as asymmetric/differential-speed rolling (ASR/DSR), accumulative roll bonding (ARB), and rolling using shear-controlled calibers—demonstrate the ability to combine high process efficiency with the effects of severe plastic deformation (SPD) [4–6].

These approaches result in the formation of ultrafine-grained and submicron structures, leading to a comprehensive enhancement of material properties. In particular, asymmetric and differential-speed rolling (ASR/DSR) accelerate dislocation accumulation and facilitate the transformation of low-angle grain boundaries into high-angle boundaries, thereby increasing yield strength and hardness while simultaneously improving plasticity—especially in aluminum and magnesium alloys [7–9]. Furthermore, the attenuation of conventional rolling textures and the introduction of shear components enhance isotropy, which is critically important for HCP (hexagonal close-packed) metals.

The accumulative roll bonding (ARB) method—based on repeated cycles of rolling and welding (stacking) metal sheets—enables the formation of nanostructured states with high strength, hardness, and fatigue resistance [10–12]. Several studies confirm this capability: ARB has demonstrated significant gains in mechanical performance due to ultrafine microstructures. The number of ARB cycles and the processing temperature critically influence the balance between strength and plasticity: while increasing the cycle count enhances grain refinement, excessive dislocation density can lead to reduced ductility [13,14].

Particularly noteworthy are rolling schemes employing non-diagonal calibers, where combined compressive and shear deformation significantly strengthens the material without sacrificing ductility. Experimental results show that such schemes can reduce grain size by more than threefold and increase tensile strength by nearly 70%, all while maintaining satisfactory plasticity [6,15,16].

Thus, modern rolling methods incorporating controlled shear deformation pave the way for the targeted improvement of metals' property complexes—from enhanced strength and hardness to improved plasticity and isotropy—making these methods highly relevant in both laboratory research and industrial applications.

2. Materials and Methods

To intensify shear deformation during rolling, the use of oval calibers whose symmetry axes are inclined relative to the longitudinal axis of the rolls has been proposed, as shown in Figure 1.

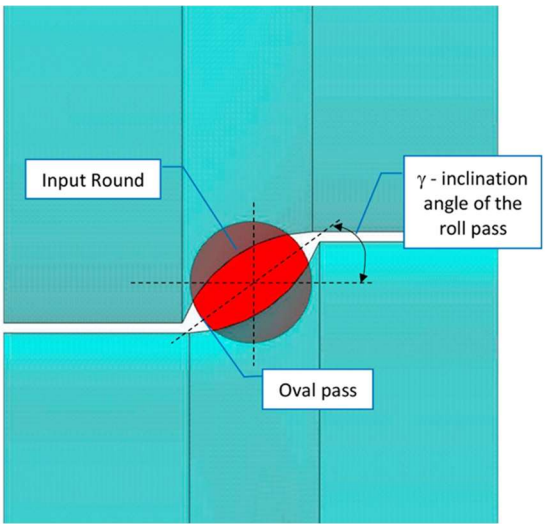


Figure 1. Schematic of an oval caliber with an inclined axis of symmetry.

In this configuration, alongside conventional reduction in height, pronounced transverse shear is activated in the deformation zone, resulting in significantly increased shear components compared to classical oval calibers. This is corroborated by analytical investigations presented in [17], where the inclination of the oval pass generates a skew-symmetric influence of the upper and lower rolls, leading to the superposition of additional shear in the deformation zone. The results of finite element method (FEM) simulations reported in [18] also confirm the realization of macro-shear deformations, which lead to an expansion of the zone of maximum strain intensity.

A sequence of alternating "oval–round" rolling passes has been devised to impart alternating-sign macro-shear deformation, comprising four consecutive passes (Figure 2). This process organization facilitates accumulation of bidirectional deformation, thereby enabling targeted control of microstructure and mechanical properties.

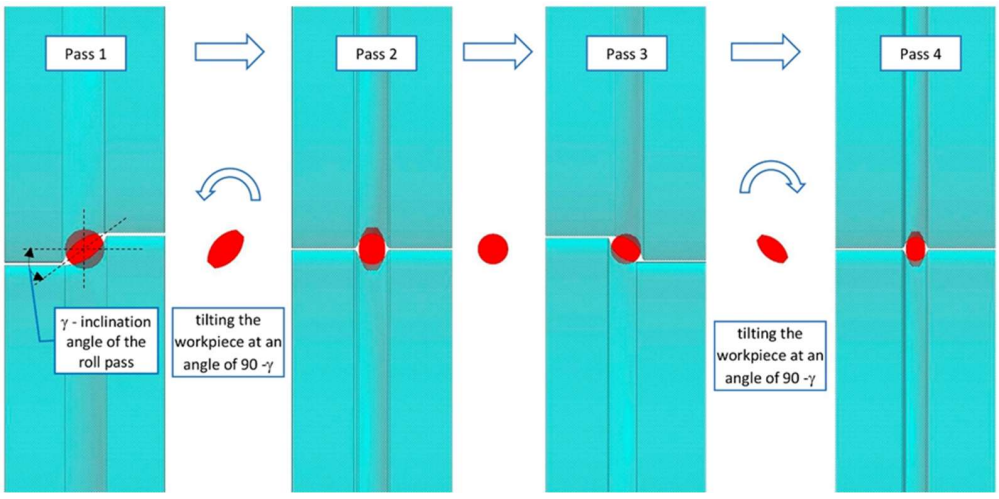


Figure 2. Roll sequence in the "oval–round" caliber system.

Experimental studies were carried out to evaluate the effect of a modified rolling scheme—incorporating inclined oval calibers—on the mechanical properties of Mn–Si low-alloy steel (Russian grade 25G2S). The chemical composition of the Russian grade 25G2S steel, based on normative sources [19], is presented in Table 1.

Table 1. Chemical composition of 25G2S steel (wt.%) [17].

C	Si	Mn	Ni (max)	S (max)	P (max)	Cr (max)	Cu (max)
0.20–0.29	0.60–0.90	1.20–1.60	≤0.30	≤0.045	≤0.040	≤0.30	≤0.30

Note: Iron (Fe) constitutes the balance of the material (≥96.2 wt.%).

For additional verification of the base material, energy–dispersive X-ray spectroscopy (EDS) was conducted using a ZEPTOOLS ZEM20 (ZepTools Technology Co., Ltd., Tongling, China) scanning electron microscope. The analysis was performed on the specimen surface after standard metallographic preparation. In the quantitative EDS analysis, carbon (C) and trace elements were deliberately excluded from the normalization in order to focus on the main alloying elements (Si, Mn). The quantification of light elements (including C) via EDS is inherently limited due to strong absorption of low-energy X-rays and contributions from surface hydrocarbon contamination; these effects can bias the normalization and matrix corrections (atomic number–absorption–fluorescence, ZAF). Therefore, compositions were calculated in the Fe–Si–Mn system, assuming "Fe as the remainder." The EDS results are shown in Figure 3 and summarized in Table 2.

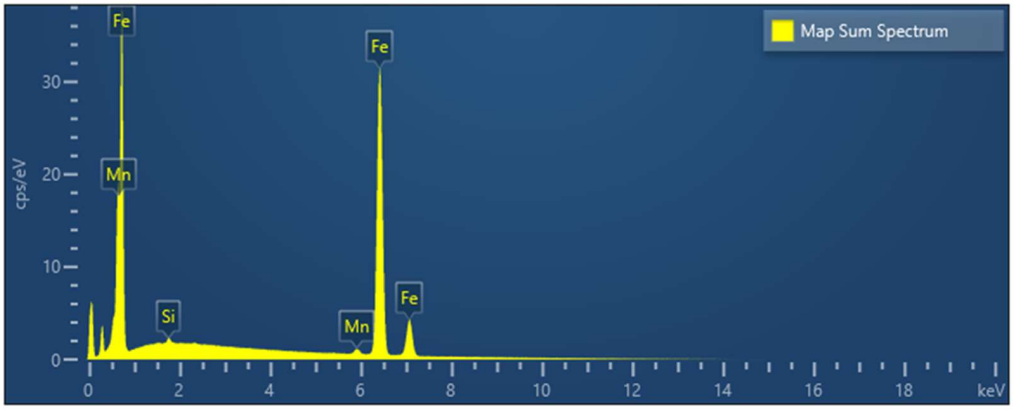


Figure 3. EDS spectrum and elemental mapping of steel 25G2S (Si, Mn, Fe).

Table 2. Results of energy-dispersive analysis of steel 25G2S (wt. %).

Element	Concentration, wt %	Uncertainty, wt %	Atomic %
Si	0.31	0.02	0.61
Mn	1.43	0.05	1.45
Fe	98.26	0.06	97.94

The average Si concentration measured (~0.31 wt %) is significantly lower than the normative range of 0.60–0.90 wt %. This discrepancy can be attributed to (i) the large relative uncertainty of EDS at low concentrations, (ii) the surface-sensitive nature of the method, (iii) possible local depletion of Si (e.g., by surface oxidation or redistribution), and (iv) effects of specimen preparation and surface geometry.

The experiments were conducted on a laboratory rolling mill (Figure 4) equipped with rollers that incorporated both classic oval calibers and modified inclined oval calibers (Figure 5), enabling a direct comparison between the two configurations. The inclination

angle of the oval caliber was set to $\gamma = 35°$, since according to the results of [18], this value provides the best balance between deformation intensity, strain uniformity, and rolling force.

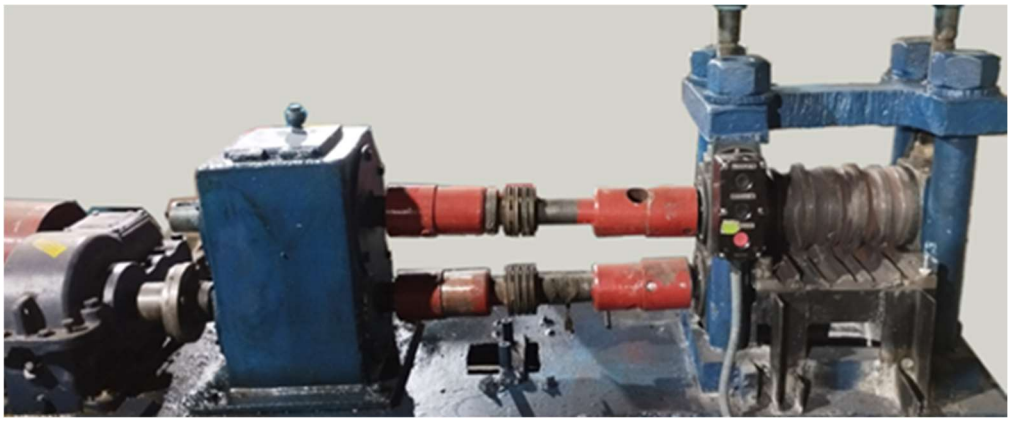


Figure 4. Laboratory rolling mill stand.

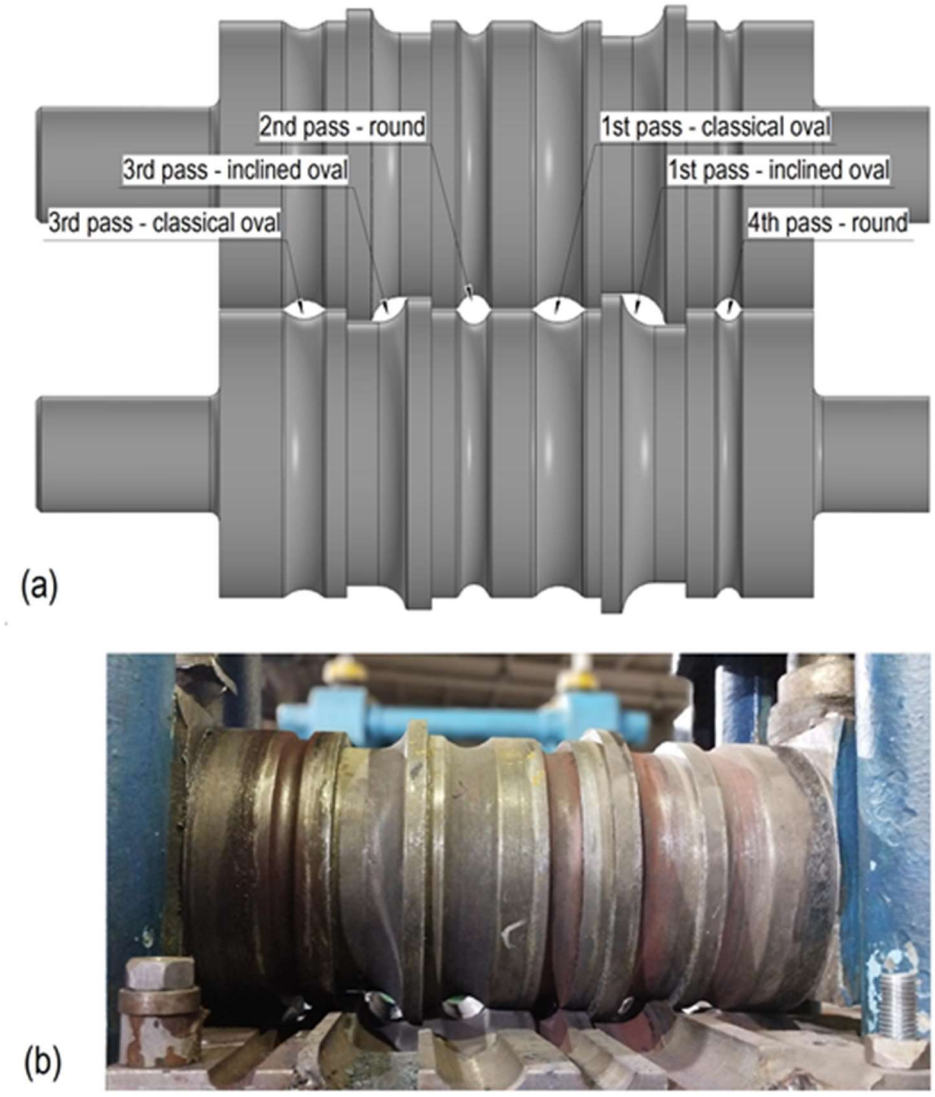


Figure 5. Design of the roll with combined classical and inclined oval passes (**a**) and installation of the roll in the laboratory stand (**b**).

Cylindrical bars measuring 20 mm in diameter and 150 mm in length were used as the starting billets. The rolling sequence comprised four consecutive passes arranged in an oval–round cycle (Figure 5a). Two schemes were tested:

- Classic scheme: traditional oval followed by round calibers.
- Modified scheme: inclined oval calibers followed by round calibers, as illustrated in Figure 2.

Prior to rolling, the billets were heated in a "Plavka.Pro PM-5" (Plavka.Pro, Korolyov, Russia) furnace to 1200 °C (Figure 6), which ensured a uniform temperature distribution across the cross-section and created favorable conditions for subsequent plastic deformation. After heating to 1200 °C, the billets were soaked in the furnace for 30 min. This soaking interval was sufficient for the given billet dimensions and steel grade, ensuring uniform temperature distribution across the cross-section and stabilization of the initial state prior to hot deformation.



Figure 6. Heating of billets to 1200 °C in the Plavka.Pro PM-5 furnace prior to rolling.

After removal from the furnace, surface scale was stripped within approximately 5 s. The working roll diameter was 150 mm, and the rolls rotated at a constant angular speed of 1.0472 rad/s. Each pass induced an elongation ratio of about 1.3, so that after four passes the final rod diameter was 12 mm. The contact time of the billet with the rolls during each pass was approximately 2–4 s, while repositioning between calibres required about 5–10 s. The total time from removing the billet from the furnace to the end of rolling was approximately 40–50 s (Figure 7). Rolling was performed under dry friction conditions without lubrication. Under these circumstances, the temperature at the end of rolling decreases only slightly, since the short contact times and overall process duration limit heat loss to the rolls and the environment. At the same time, plastic work and internal friction produce adiabatic heating, which compensates for part of the thermal drop. Previous studies [20,21] have demonstrated that for short-duration hot rolling the temperature drop is minor relative to the heating inputs. Both schemes produced final rod diameters of 12 mm (Figure 8).

Tensile tests were carried out at room temperature using a WDW-100 universal electromechanical testing machine (Jinan Xinguang Test Machine Manufacturing Co., Ltd., Jinan, China) with 100 kN capacity, in accordance with ISO 6892-1 (Figure 9). The crosshead speed was set to 1.5 mm/min [22]. Specimens were machined to the geometry shown in Figure 10, with an original gauge (parallel) length of approximately 40 mm. No extensometer was used during the tests. Instead, total elongation after fracture was determined by measuring the gauge length between marks placed before testing and the final gauge

length of the broken specimen. Reduction in area was determined by measuring the smallest cross-sectional area at the neck after fracture.



Figure 7. Experimental hot rolling of a red-hot billet through oval and round calibers.

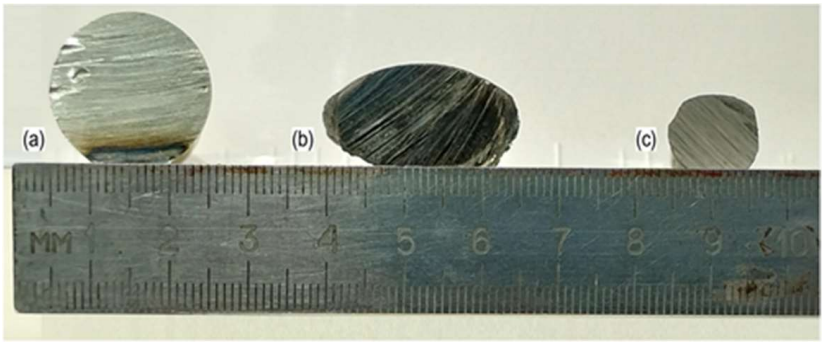


Figure 8. Cross-sections of samples: (**a**) initial, (**b**) after one pass, and (**c**) after four passes of rolling using the new "oval–round" pass design.



Figure 9. Tensile testing on a WDW-100 universal testing machine.

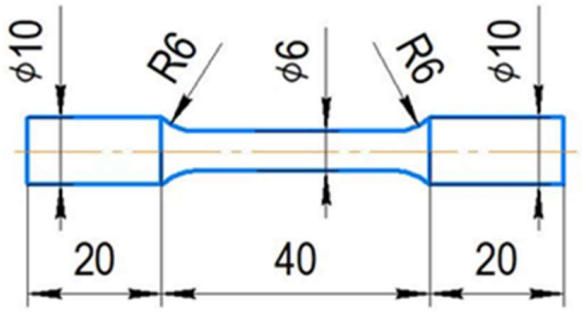


Figure 10. Geometry and dimensions of the tensile specimen.

Because no extensometer was used, parameters that depend on precise strain measurement in the elastic and early plastic regions—such as conventional 0.2% proof strength and modulus of elasticity—have greater uncertainty in our results. However, for materials that show a distinct yield plateau, the upper and lower yield points (Figure 11), tensile (ultimate) strength, total elongation, and reduction in area can be reliably reported using this manual, post-fracture measurement method.

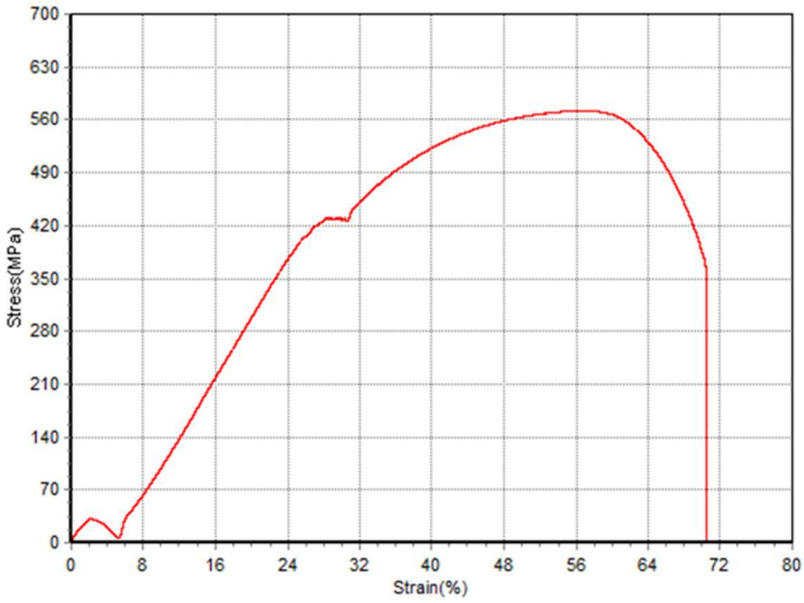


Figure 11. Stress–strain curve of a modified-rolled specimen, showing a distinct yield plateau with upper and lower yield points.

Hardness measurements were conducted using a Vickers microhardness tester HVT-1000A (Laizhou Laihua Testing Instrument Factory, Laizhou, China), with 10 indentations per sample to ensure statistical reliability. A test force consistent with microhardness protocols was applied (200 gf), and after a dwell time of 10–15 s, the diagonals of each indentation were optically measured at magnifications of 100× (Figure 12). The Vickers hardness (HV) was automatically calculated based on the average diagonal length. Indentations were spaced at least three times the mean diagonal length apart, in accordance with ISO 6507-1 [23].

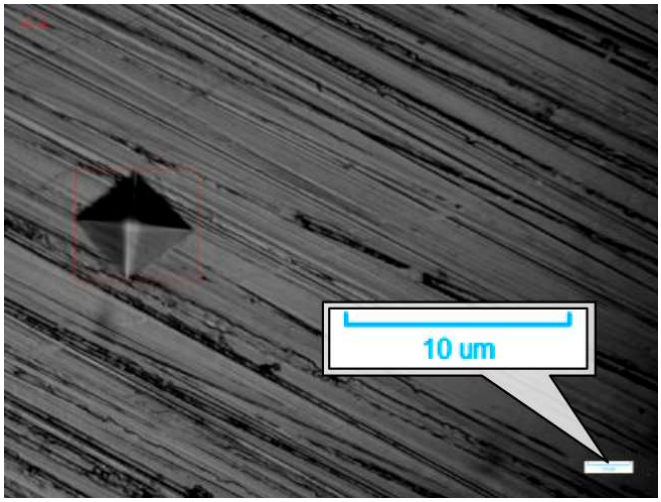


Figure 12. Micrograph of the indent area.

To evaluate the effect of rolling technology on structure formation, metallographic examinations were carried out. Specimens of 25G2S steel were extracted from bars in two orientations—transverse and longitudinal—taken from the mid-length region at approximately half-radius (≈1/2R). Coupons were sectioned, orientation-marked, and cold mounted in epoxy (Figure 13). Surface preparation followed a standard metallographic procedure involving mechanical grinding, fine polishing, and brief chemical or electrochemical etching to reveal grain boundaries; surfaces were then rinsed and dried. No conductive coating was required due to the electrical conductivity of the steel. Scanning electron microscopy was performed on a ZEPTOOLS ZEM20 in secondary-electron (SE) mode under high vacuum at a nominal magnification of ×5000 with a 10 µm scale bar (Figure 14). Images were acquired using typical accelerating-voltage and working-distance settings for steel, selecting representative areas away from edges and visible defects, and saved in JPEG format (highest-quality setting).

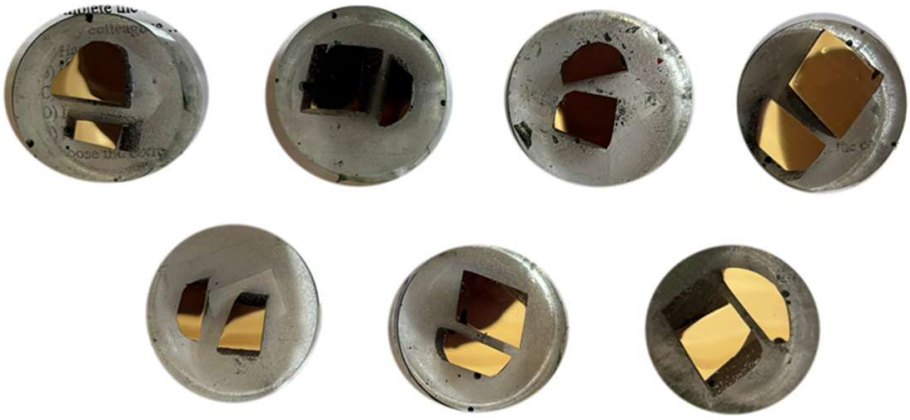


Figure 13. 25G2S steel coupons (transverse and longitudinal sections, mid-length at ≈1/2R) cold-mounted in epoxy.



Figure 14. ZEPTOOLS ZEM20 scanning electron microscope.

3. Results and Discussion

The results obtained from tensile testing are presented in Table 3.

The mechanical properties obtained from tensile testing under the three processing states—initial (unrolled), classical rolling, and modified rolling—are summarized in Table 4. For each condition, the results are presented as average ± SD, based on 4 specimens for the initial and classical-rolled states, and 7 specimens for the modified-rolled state..

Table 3. Results of tensile testing using universal machine WDW-100.

Condition	Sample	Yield Strength, MPa	Ultimate Tensile Strength, MPa	Elongation at Break, %	Reduction in Area, %
Initial (unrolled)	1	293.5	502	21.95	66.37
	2	269	492	24.39	64.2
	3	272.5	504	21.95	61.15
	4	258.5	477	25	61.56
Classical rolling	1	434	577	23.81	68.18
	2	475.5	593	21.43	67.84
	3	441.5	590	21.43	63.73
	4	424.5	577	29.27	69.62
Modified rolling	1	444	579	24.39	69.2
	2	419.5	572	23.81	71.3
	3	435	589	24.39	67.61
	4	459.5	571	30.95	65.96
	5	448.5	583	26.83	68.61
	6	404.5	545	27	70.84
	7	402.5	574	25.55	70.58

Table 4. Mechanical properties from tensile testing for initial, classical-rolled, and modified-rolled specimens (mean ± SD).

Condition	Yield Strength, MPa	Ultimate Tensile Strength, MPa	Elongation at Break, %	Reduction in Area, %
Initial (unrolled)	(268.6 ± 14.3)	(493.8 ± 12.6)	(23.32 ± 1.29)	(63.32 ± 2.15)
Classical rolling	(443.9 ± 22.3)	(584.3 ± 6.8)	(24.48 ± 3.14)	(67.84 ± 2.47)
Modified rolling	(433.0 ± 20.8)	(572.4 ± 15.7)	(26.81 ± 2.49)	(68.61 ± 1.85)

Relative to the initial (unrolled) material, the classical rolling scheme significantly increased the yield strength by about 62% (from ~269 MPa to ~444 MPa on average) and the ultimate tensile strength by about 19% (from ~494 MPa to ~584 MPa). Ductility, as measured by elongation at break, was only modestly changed (from ~23.3% in the initial state to ~24.5% after classical rolling), while reduction in cross-sectional area increased slightly (~4 percentage points). Under the modified rolling scheme, the strength metrics remain close to those achieved under the classical approach (average yield ~433 MPa, ultimate ~572 MPa), but ductility improved further (average elongation ~26.8%) and reduction in area rose to ~68.6%. This favorable trade-off—i.e., enhanced plasticity without serious loss in strength—suggests the activation of softening microstructure mechanisms intrinsic to hot deformation, particularly dynamic recovery and dynamic recrystallization. These mechanisms promote the formation of new, low-strain grains and reduce dislocation density, thereby refining the microstructure and enabling more uniform deformation with lower work hardening rate and lower hardness [24,25].

We emphasize that the summary data are descriptive. Because only arithmetic means and standard deviations are reported, it remains possible that some of the observed differences (particularly in ductility) arise from sample scatter. Though we do not present formal significance tests here, the overlap of the confidence intervals (mean ± standard deviation) suggests that not all differences may reach statistical significance. Meanwhile, the consistent trends across multiple specimens support the reliability of our conclusions about the beneficial balance achieved via the modified rolling scheme.

In Table 5 are presented the Vickers hardness results for the three conditions: initial (unrolled), after classical rolling, and after modified rolling, now including both the mean values and the standard deviation over 10 indents per sample.

Table 5. Vickers microhardness results for initial, classical-rolled, and modified-rolled conditions (mean ± SD, 10 indents per sample).

Indentation No.	Vickers Hardness		
	Initial (Unrolled)	Classical Rolling	Modified Rolling
1	262.7	211.1	174
2	230.8	227.3	185.4
3	224.8	206.6	184.1
4	223.9	211.1	184.8
5	223.9	202.2	179.2
6	244.5	212.7	182.9
7	252.3	208.8	186.7
8	268	229.9	185.4
9	263.7	214.2	187.9
10	245.5	211.1	179.2
Mean ± SD	(244.0 ± 17.7)	(213.5 ± 9.1)	(183.6 ± 4.8)

In Table 5, the average hardness of the un-rolled (initial) material is approximately 244.0 HV with a standard deviation of 17.7 HV. After classical rolling, the average drops to ~213.5 HV with a SD of 9.1 HV, whereas the modified rolling yields an average hard-ness of ~183.6 HV with a much tighter scatter of ±4.8 HV. This reduction in scatter strengthens the claim that the modified rolling promotes structural uniformity, in addition to lowering average hardness. Similar observations have been reported in the context of hot rolling processes where shear-imparted deformation refines grain structure and homogenizes mechanical response [26].

Figure 15 presents SEM micrographs of the microstructure of 25G2S steel in the as-received condition and after classical and modified rolling (tilted oval caliber), acquired in secondary-electron (SE) mode at 5000× with a 10 μm scale bar on a ZEPTOOLS ZEM20 microscope.

After hot rolling followed by air cooling, all conditions exhibit the characteristic ferrite–pearlite aggregate of a low-carbon Mn–Si steel. In the as-received material, pearlite colonies are comparatively coarse and distributed non-uniformly, while the ferritic matrix displays an irregular polygonal morphology; the apparent ferrite grain size is ~6–10 μm in the transverse section (Figure 15a) and ~7–12 μm in the longitudinal section (Figure 15b). Throughout this work, grain sizes are interpreted as "apparent" values in the sense of ISO 643/ASTM E112, i.e., derived from revealed grain boundaries on 5000× micrographs and reported as ranges over the observed fields.

The classical oval-round sequence produces marked refinement in the transverse section: the apparent ferrite grain size decreases to ~2–4 μm and pearlite colonies disperse to ~3–6 μm (Figure 15c). In the longitudinal section, a coarser cell of ~4–6 μm persists together with faint vestiges of inherited banding and oriented contrast (Figure 15d). This anisotropy is consistent with a predominantly symmetric strain path during rolling and with the well-known outcome of recovery/recrystallization during hot deformation of low-carbon steels, whereby equiaxed grains coarsen in the bulk while oriented elements may partially persist along the rolling direction [27].

In the modified sequence employing a tilted oval caliber, refinement in the transverse section is comparable (~3–5 μm) (Figure 15e), whereas the most pronounced differences emerge in the longitudinal section, where the apparent ferrite grain size is ~3–5 μm and the banded contrast is attenuated (Figure 15f). This points to an altered deformation route with an increased shear component γ introduced by the tilt, which creates a skewed contact zone and through-thickness gradients of friction/pressure. Literature on asymmetric (shear-assisted) rolling consistently shows that additional shear promotes dynamic/metadynamic recrystallization, raises the fraction of high-angle boundaries, and favors a finer, more isotropic ferritic morphology—effects that are particularly evident in the longitudinal orientation. The observed dispersion and weakening of texture-related contrast are fully consistent with this mechanism [8,28].

The resulting morphology aligns with the previously presented mechanical trends: ferrite grain refinement together with a rationalized pearlite topology accounts for strength elevation via Hall–Petch scaling, while shear-assisted redistribution of strain under the tilted caliber yields a more spatially uniform structure (across area and thickness), consistent with an improved ductility balance and a reduced mean and scatter of microhardness.

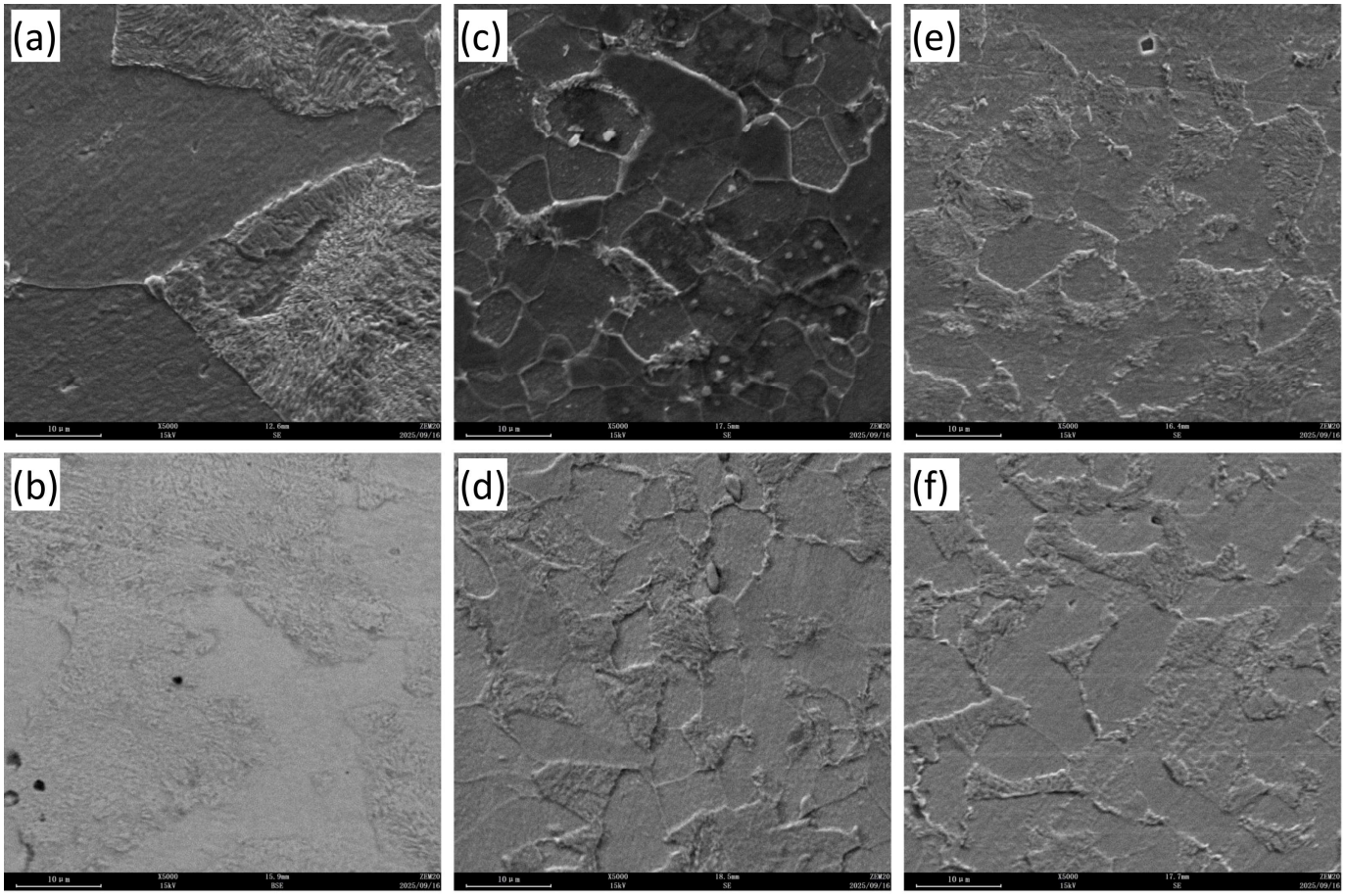


Figure 15. SEM micrographs of the microstructure of 25G2S steel (SE mode, 5000×, 10 μm scale bar): (**a**) transverse, as-received; (**b**) longitudinal, as-received; (**c**) transverse after classical rolling; (**d**) longitudinal after classical rolling; (**e**) transverse after modified rolling; (**f**) longitudinal after modified rolling.

4. Conclusions

1. Strength–ductility balance: Classical oval–round rolling enhanced the strength of 25G2S steel by raising $\sigma_{0.2}$ to ~444 MPa and σ_v to ~584 MPa, while the modified (inclined) scheme retained comparable strength (~433 and ~572 MPa, respectively). At the same time, the modified route provided superior ductility, with elongation exceeding 26% and reduction in area approaching 69%, highlighting its advantage in achieving a more favorable mechanical balance.
2. Hardness evolution and uniformity: Both rolling schemes reduced Vickers hardness relative to the as-received state (244 HV → 213 HV for classical, 184 HV for modified). Notably, the modified path minimized scatter (±4.8 HV), which signifies improved structural uniformity and reproducibility of properties across the section.
3. Microstructural refinement: SEM micrographs confirmed significant grain refinement in all rolled states. In particular, the modified scheme led to equiaxed ferrite grains of 3–5 μm and suppressed banding in the longitudinal section, indicative of enhanced isotropy. Such morphological features are consistent with active dynamic and metadynamic recrystallization triggered by shear-assisted deformation.
4. Shear-driven mechanism: The introduction of tilted oval calibers modifies the strain path, superimposing shear on the deformation field. This raises the effective strain and accelerates subgrain boundary formation, thereby promoting DRX kinetics. The observed microstructural changes directly support this mechanistic interpretation.

5. Technological significance: The modified oval–round rolling scheme provides an efficient pathway to tailor mechanical response via controlled microstructural refinement. The method offers practical potential for industrial-scale rolling operations, where improved ductility, structural homogeneity, and reliable strength are critical performance targets.

Author Contributions: K.N.: conceptualization; methodology; investigation; writing—original draft preparation; visualization. M.A.: methodology; formal analysis; investigation. Z.A.: investigation; formal analysis; methodology. G.A.: methodology; investigation; formal analysis; data processing. S.K.: methodology; formal analysis; data processing. I.T.: investigation; writing—review and editing. All authors have read and agreed to the published version of the manuscript.

Funding: This research has is funded by the Science Committee of the Ministry of Science and Higher Education of the Republic of Kazakhstan (Grant No. AP19674502).

Institutional Review Board Statement: Not applicable.

Informed Consent Statement: Not applicable.

Data Availability Statement: The original contributions presented in this study are included in the article. Further inquiries can be directed to the corresponding author.

Conflicts of Interest: The authors declare no conflicts of interest.

References

1. Valiev, R.Z.; Islamgaliev, R.K. Enhanced Superplasticity of Ultrafine-Grained Alloys Processed by Severe Plastic Deformation. *Mater. Sci. Forum* **1999**, *304*, 39–46. [CrossRef]
2. Zhilyaev, A.P.; Langdon, T.G. Using High-Pressure Torsion for Metal Processing: Fundamentals and Applications. *Prog. Mater. Sci.* **2008**, *53*, 893–979. [CrossRef]
3. Segal, V.M. Review: Modes and Processes of Severe Plastic Deformation (SPD). *Materials* **2018**, *11*, 1175. [CrossRef]
4. Ji, Y.H.; Park, J.J. Development of Severe Plastic Deformation by Various Asymmetric Rolling Processes. *Mater. Sci. Eng. A* **2009**, *499*, 14–17. [CrossRef]
5. Dhinwal, S.S.; Toth, L.S.; Hodgson, P.D.; Haldar, A. Effects of Processing Conditions on Texture and Microstructure Evolution in Extra-Low Carbon Steel during Multi-Pass Asymmetric Rolling. *Materials* **2018**, *11*, 1327. [CrossRef] [PubMed]
6. Naizabekov, A.B.; Bykhin, M.B.; Nogaev, K.A.; Bykhin, B.B. Study of the Process of Realization of High-Rate Plastic Deformation in Lengthwise Rolling. In Proceedings of the 19th International Conference on Metallurgy and Materials (METAL 2010), Brno, Czech Republic, 19–21 May 2010; pp. 192–202. Available online: https://www.confer.cz/metal/2010 (accessed on 2 September 2025).
7. Vincze, G.; Simões, F.J.P.; Butuc, M.C. Asymmetrical Rolling of Aluminum Alloys and Steels: A Review. *Metals* **2020**, *10*, 1126. [CrossRef]
8. Ren, X.; Huang, Y.; Zhang, X.; Li, H.; Zhao, Y. Influence of Shear Deformation during Asymmetric Rolling on the Microstructure, Texture, and Mechanical Properties of the AZ31B Magnesium Alloy Sheet. *Mater. Sci. Eng. A* **2021**, *800*, 140306. [CrossRef]
9. Godec, M.; Kralj, D.; Kosec, B.; Kolar, M.; Kosec, M. Influence of Symmetric and Asymmetric Rolling on Texture and Deep Drawing Properties of Aluminum Alloys. *Trans. Nonferrous Met. Soc. China* **2025**, *35*, 473–483. [CrossRef]
10. Ghalehbandi, S.M.; Malaki, M.; Gupta, M. Accumulative Roll Bonding–A Review. *Appl. Sci.* **2019**, *9*, 3627. [CrossRef]
11. Ghaderi, O.; Zare, M.; Sadabadi, H.; Toroghinejad, M.R.; Najafizadeh, A.; Church, B.C.; Rohatgi, P.K. Structural and Mechanical Properties of Cu-SiCp Nanocomposites Fabricated by Accumulative Roll Bonding (ARB). *Front. Mater* **2024**, *11*, 1362746. [CrossRef]
12. Roy, S.; Singh, S.D.; Suwas, S.; Kumar, S.; Chattopadhyay, K. Evolution of Texture and Microstructure during Accumulative Roll Bonding of Aluminum AA5086 Alloy. *Mater. Sci. Eng. A* **2011**, *528*, 8469–8474. [CrossRef]
13. Ebrahimi, M. Accumulative Roll-Bonding of Aluminum Alloys and Composites: A Review. *J. Mater. Res. Technol.* **2022**, *18*, 348–369. [CrossRef]
14. Sivakumar, K.; Ramesh, K.; Suresh, S.; Rajendran, I.; Ramesh, R. Review on Accumulative Roll Bonding (ARB) Techniques for Improving the Mechanical Properties of Multi-Layered Materials. *J. Mater. Sci. Technol.* **2020**, *56*, 1–15. [CrossRef]
15. Abishkenov, M.; Ashkeyev, Z.; Nogaev, K. Investigation of the Shape Rolling Process Implementing Intense Shear Strains in Special Diamond Passes. *Materialia* **2022**, *26*, 101573. [CrossRef]

16. Ashkeyev, Z.; Abishkenov, M.; Nogaev, K.; Bestembek, Y.; Azimbayev, K.; Tavshanov, I. Stress State of Workpieces during Upsetting with Additional Shear. *Eng. Solid Mech.* **2023**, *11*, 253–262. [CrossRef]
17. Nogayev, K.; Abishkenov, M.; Tavshanov, I.; Ashkeyev, Z.; Kunaev, V.; Akhmetova, G.; Kamarov, A. Enhanced Shear De-formation in Rod Rolling with Inclined Oval Pass Modification. *Acta Metall. Slovaca* **2025**, *31*, 186–193. [CrossRef]
18. Nogayev, K.; Kamarov, A.; Abishkenov, M.; Ashkeyev, Z.; Sembayev, N.; Kydyrbayeva, S. Finite Element-Based Multi-Objective Optimization of a New Inclined Oval Rolling Pass Geometry. *Modelling* **2025**, *6*, 110. [CrossRef]
19. Steel-Grades. GOST 25G2S—Chemical Composition and Mechanical Properties of Steel Grade 25G2S. Available online: https://www.steel-grades.com/metals/85/211097/GOST-25G2S.html (accessed on 6 September 2025).
20. Zhao, X.; Chen, L.; He, K.; Wu, N.; Zeng, J. Effect of Contact Heat Transfer on Hot Rolling of Aluminum Alloy. *Procedia Manuf.* **2019**, *37*, 91–96. [CrossRef]
21. Speicher, K.; Steinboeck, A.; Wild, D.; Kiefer, T.; Kugi, A. An Integrated Thermal Model of Hot Rolling. *Math. Comput. Model. Dyn. Syst.* **2014**, *20*, 66–86. [CrossRef]
22. Baciu, F.; Rusu-Casandra, A.; Pastramă, Ş.-D. Low Strain Rate Testing of Tensile Properties of Steel. *Mater. Today: Proc.* **2020**, *32*, 128–132. [CrossRef]
23. *ISO 6507-1:2023*; Metallic Materials—Vickers Hardness Test—Part 1: Test Method. ISO: Geneva, Switzerland, 2023.
24. Derazkola, H.A.; García Gil, E.; Murillo-Marrodán, A.; Méresse, D. Review on Dynamic Recrystallization of Martensitic Stainless Steels during Hot Deformation: Part I—Experimental Study. *Metals* **2021**, *11*, 572. [CrossRef]
25. Montheillet, F. Dynamic Recrystallization Behaviours in Metals and Alloys. *Materials* **2023**, *16*, 976. [CrossRef] [PubMed]
26. Varela-Castro, G.; Cabrera, J.-M.; Prado, J.-M. Critical Strain for Dynamic Recrystallisation. The Particular Case of Steels. *Metals* **2020**, *10*, 135. [CrossRef]
27. Hwang, J.-K. Hardening and Softening Behavior of Caliber-Rolled Wire. *Materials* **2022**, *15*, 2939. [CrossRef]
28. Zhang, T.; Li, L.; Lu, S.-H.; Gong, H.; Wu, Y.-X. Comparisons of Different Models on Dynamic Recrystallization of Plate during Asymmetrical Shear Rolling. *Materials* **2018**, *11*, 151. [CrossRef]

Disclaimer/Publisher's Note: The statements, opinions and data contained in all publications are solely those of the individual author(s) and contributor(s) and not of MDPI and/or the editor(s). MDPI and/or the editor(s) disclaim responsibility for any injury to people or property resulting from any ideas, methods, instructions or products referred to in the content.